Design Optimization of a Differential Piston Warm Gas Self-Pressurization System*

FANG Zhong-jian，LIANG Guo-zhu

（School of Astronautics，Beijing University of Aeronautics and Astronautics，Beijing 100083，China）

Abstract：In order to obtain the optimal design of a differential piston warm gas self-pressurization system for the liquid attitude and divert propulsion system，an approach for design optimization through genetic algorithm is discussed. The system includes the solid start cartridge，pressure amplified tank with liquid monopropellant，liquid regulator，gas generator，pipes. The multi-objective constrained optimization is aimed at the system total mass and starting time minimization with given requirements，constraints and design assumptions. Evaluation modules are developed to estimate the system total mass，the axial dimension，the radial dimension and the system performance parameters. The weighted sum method and penalty function method as well as the genetic algorithm are utilized to solve the multi-objective constrained optimization. According to the Pareto-frontier solutions，the optimized results can be obtained，whereas the weighted factor of the system total mass varies within [0.4，1.0]. The single-objective optimizations are executed to obtain the optimal value of each system parameter，the system total mass，the starting time，the centroid drift，the axial dimension and the radial dimension can be respectively decreased 23.17%，34.40%，84.10%，62.28% and 4.14%，and the pressurization efficiency can be increased 0.42%. The design variables effects on the system parameters are also investigated. These parameters are mainly affected by the gas cavity initial volume，the liquid cavity diameter of the pressure amplified tank and the solid propellant mass of the start cartridge.

Key words：Differential piston；Warm gas self-pressurization system；Liquid attitude and divert propulsion system；Multi-objective optimization；Genetic algorithm

CLC number：V434^{+}.23 **Document code**：A **Article number**：1001-4055（2018）08-1905-16

DOI：10.13675/j. cnki. tjjs. 2018. 08. 027

差动活塞式热气自增压系统优化设计*

方忠坚，梁国柱

（北京航空航天大学 宇航学院，北京 100083）

摘　要：为了进行应用于液体姿轨控动力系统的差动活塞式热气自增压系统优化设计，研究了一种基于遗传算法的优化设计方法。该系统由起动药盒、压力放大贮箱、流量调节器、燃气发生器和管道等组成。文中提出了在给定要求、约束和假设条件下进行系统总质量和起动时间的有约束多目标优化任务；建立了系统总质量、轴向尺寸、径向尺寸和系统性能参数的计算模型；采用归一加权法、惩罚函数法以及遗传算法求解了有约束多目标优化问题。根据帕累托前沿解，系统总质量的加权因子在[0.4，1.0]内变化时，可以得到优化结果。为了得到系统参数作为单目标的优化结果，本文进行了系统单目标优化，系统总质量、起动时间、质心漂移、轴向尺寸和径向尺寸各自作为优化目标可分别降低23.17%，34.40%，84.10%，62.28%和4.14%，增压效率可提高0.42%。分析了设计变量对系统参数的

---

* 收稿日期：2017-12-03；修订日期：2018-01-31。
作者简介：方忠坚，男，博士生，研究领域为液体姿轨控动力系统。E-mail: fzj4919@163.com
通讯作者：梁国柱，男，博士，教授，研究领域为火箭发动机。E-mail: lgz@buaa.edu.cn

影响，结果表明压力放大贮箱气体腔初始体积、液体腔直径和起动药盒固体推进剂质量是影响系统参数的主要设计变量。

关键词：差动活塞；热气自增压系统；液体姿轨控动力系统；多目标优化；遗传算法

Nomenclature

m	Mass, kg	K	Spring stiffness, N/m
t	Time, s	q_m	Mass flow rate, kg/s
p	Pressure, Pa	C_d	Flow coefficient
ρ	Density, kg/m^3	c	Circumference, m
T	Temperature, K	H	Flow resistance coefficient
V	Volume, m^3	Re	Reynolds number
k	Specific heat ratio	L_r	Radial dimension, m
u	Velocity, m/s	L_a	Axial dimension, m
A	Area, m^2	M	Mass, kg
Q_T	Quantity of heat, J	n	Number
S	Heat transfer area, m^2	h	Specific enthalpy, J/mol
F	Force, N	Δ	Thickness, m
L	Length, m	C	Damping coefficient
D	Diameter, m	x	Displacement, m
l	Regulator opening, m	η	Pressurization efficiency
a_l	Liquid sound speed, m/s	ξ	Excretion rate of the PAT monopropellant
h_s	Convective heat transfer coefficient, W/(m^2·K)	a_s	Specific surface area of catalyst bed, m^2/ m^3
$[\sigma]$	Pressure intensity of wall material, Pa	G_b	Bed flux of catalyst bed, kg/(m^2·s)
ε	Porosity of catalyst bed		

Subscripts

p	Solid propellant	w	Wall
eb	End-burning	pst	Piston
ib	Internal-burning	f	Friction
g	Gas	i	Inlet cavity
l	Liquid	o	Outlet cavity
reg	Liquid regulator	GG	Gas generator
regc	Valve core of liquid regulator	SC	Start cartridge
a	Ambient	PAT	Pressure amplified tank
PT	Propellant tank	st	Starting time
in	Inlet	off	Self-locking state
out	Outlet	0	Initial state
inj	Injector	max	Maximum
cb	Catalyst bed	mop	Monopropellant
ctl	Catalyst	tub	Tubular wall
pi	Pipe	eh	Wall of ellipsoidal head
co	Wall of cone	bot	Wall of flat bottom
a	Axial direction	F	Final
r	Radial direction	b	Boundary
cpl	Capillary	oth	Other

1 Introduction

The function of the differential piston warm gas self-pressurization system (DPWGSPS) is to generate warm gas for tank pressurization via catalytic chemical reactions of the liquid monopropellant for the liquid attitude and divert propulsion system. The use of a DPWGSPS can significantly reduce both weight and the volume, eliminate the stored gas, as well as to enhance safety and reliability in comparison with the cold gas pressurization system[1]. The technology has attracted attention in recent years as a candidate for a number applications including rockets, spacecraft and missiles.

A monopropellant DPWGSPS applying M-75 (hydrazine/MMH blend) was developed and tested in 1998 by the Primex Aerospace Company, which was designed to pressurize propellant tanks and provided a regulation band of $5.8\text{MPa}^{+5\%}_{-7\%}$[1]. Further to this, a parameter design method on the DPWGSPS was developed by the authors[2,3]. The DPWGSPS has several advantages over typical propulsion systems such as improved pressurization efficiency, low system mass, and small envelope size[4].

For the multi-objective optimization (MOO) of liquid propellant rocket engines, Cai et al[5,6] utilized variable weight method, e-Constraint method, and neighborhood cultivation genetic algorithm to obtain the Pereto frontier solutions in the multi-objective processing to maximization of the engine specific impulse and the thrust to weight ratio. Kosugi et al[7] applied the multi-objective genetic algorithm and a data mining technique to the optimization of a hybrid rocket, utilizing real-number cording and the Pareto ranking method to solve the multi-objective problem. Oyama and Liou[8] proposed a multi-objective evolutionary algorithm for the optimization of cryogenic rocket engines turbopumps. Zheng et al[9] established a system simulation model and a MOO model for the single gas generator cycle system. Zhang et al[10] introduced a MOO of a liquid propellant rocket engine through both hybrid and genetic algorithms. Pastrone et al[11] investigated a MOO of a rocket based combined engine through a hybrid evolutionary algorithm. In contrast, the researches on the design optimization of DPWGSPS rarely exist. In order to guide further system design and test, it is necessary to conduct the system design optimization. The methods in aforementioned references, such as the genetic algorithm and the variable weight method are useful for current research.

Therefore, the purpose of the present work is to develop an approach for design optimization through the genetic algorithm of the DPWGSPS. Evaluation modules are developed to estimate the system parameters. The weighted sum method, the penalty function method and the genetic algorithm are utilized to solve the multi-objective constrained optimization. The design variables effects on the system parameters are investigated through these evaluation modules. The multi-objective constrained optimization is aimed at the system total mass and starting time minimization with given requirements, constraints and design assumptions through the design variables changes. The single-objective optimizations are also executed to obtain the optimal value of each system parameter.

2 System model

The DPWGSPS schematic is presented in Fig. 1. It consists of a start cartridge (SC), a pressure amplified tank (PAT), a liquid regulator (LR), a gas generator (GG), a check valve (CV), burst disks (BD) and pipelines.

2.1 Design model

The system design model includes system parameter design and system layout design. The system parame-

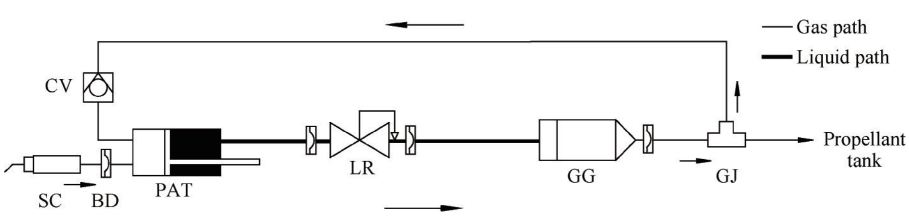

Fig. 1 Schematic diagram of the differential piston warm gas self-pressurization system

ter design is the basis of system optimization. The purpose of the calculation is to obtain the overall parameters on the foundation of system requirements and optimized design variables given through the optimization process, providing the known parameters for the calculations of the system total mass and the system performance parameters. The system layout design is to determine the spatial layout and the positional relationship between the system components, and then to provide the basis for the system structure size and the system centroid drift calculation. The ammonium nitrate propellant and the hydrazine 70 are respectively selected in the SC and the PAT, whereas the demand of the propellant tank (PT) pressure is 6.90MPa.

2.1.1 Parameter design

In the optimization process, the system parameter design is based on the optimized design variables for the known parameters. The detailed design model for the parameters calculation of the system is provided in Ref. [2]. The mass of the solid propellant charge, the initial volume of gas cavity and the pressure drop of the LR are the important parameters involved in this paper, so they are described in detail.

The solid propellant charge of the SC, as presented in Fig.2, is composed of an end-burning grain and an internal-burning tubular grain. This design could demonstrate fast response, lower pressure peak and sustainable pressure. The mass of the solid propellant charge can be expressed as

$$m_p = \rho_p (A_{eb} L_{eb} + A_{ib} L_{ib}) \tag{1}$$

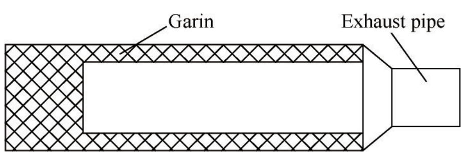

Fig. 2 Schematic diagram of the start cartridge

For the PAT, as presented in Fig.3, the corresponding initial volume of gas cavity V_{g0} can be calculated as follows

$$V_{g0} = L_{g0} \cdot \frac{\pi}{4} d_g^{\ 2} \tag{2}$$

For the DPWGSPS, the pressure of the PAT liquid cavity p_l can be expressed as

$$p_l = \Delta p_{reg} + \Delta p_{oth} + p_{PT} \tag{3}$$

The Δp_{oth} is the pressure drop of other components except LR of the flow path from the PAT to the PT. From the equation, it is clear that the value of the pressure drop Δp_{reg} of the LR has a direct effect on the pressure of the PAT liquid cavity, which affects the system pressure distribution and constitutes an important design parameter.

After the system parameter design, the system structure layout, the system total mass and the system performance parameters can be calculated by using the obtained design parameters.

2.1.2 Structure layout

The main components of the system are arranged in the axial direction, as presented in Fig.4. From the layout, the system radial dimension is determined by the PAT gas cavity diameter, whereas the system axial dimension is decided by the lengths of PAT, LR, GG and these connecting pipes between them.

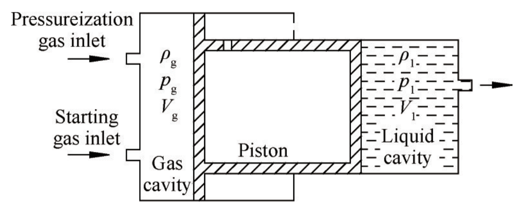

Fig. 3 Schematic diagram of the pressure amplified tank

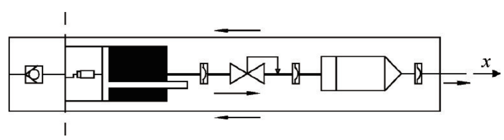

Fig. 4 Layout of DPWGSPS

Subsequently to the DPWGSPS layout finished, according to the overall requirements of the propulsion system, the overall boundary dimension can be calculated. The system can be regarded as two-dimension configuration in accordance with the symmetry. The overall boundary dimension can be divided into the radial and axial directions, as follows

$$L_r = \sum L_{r,i} \tag{4}$$

$$L_a = \sum L_{a,i} \tag{5}$$

2.2 System performance parameter evaluation

System starting time, centroid drift and pressurization efficiency are important parameters to evaluate system performance, they can be defined as the performance parameters. For the system, short starting time, small centroid drift and large pressurization efficiency are general requirements, and the starting time, the centroid drift and the pressurization efficiency can be selected as the system's optimization objectives or constraints.

2.2.1 Starting time evaluation

The starting time is one of the mainly indexes of the system, which can be defined as the time from the system start to the moment of the PAT gas cavity pressure being equal to the pressure of the propellant tank, where the system reaches self-locking at that moment. The calculation of starting time requires dynamic simulation of the system starting process. Also, the system dynamic model consists of sub-models of the pipe, the vessel, the PAT, the LR, the GG, and the SC.

The system starting process includes the sub-processes of pipe filling, gas pipe and liquid pipe flows. Therefore, the dynamic sub-models of the gas pipe, the liquid pipe and the filling pipe are required to be established, whereas the finite-element state-variables model of one-dimensional flow can be adopted, which is introduced in Ref. [12]. Moreover, as for the single volume vessel, which has multi-inlet and multi-outlet, the lumped parameter dynamic model can be utilized as described in Ref. [12].

The PAT consists of a removable piston, a variable-volume gas cavity and a liquid cavity, as presented in Fig. 3, constituting a unique new component of DPW-GPS. The dynamic operation process includes the mass-increasing and volume-increasing processes in the gas cavity, the mass-decreasing and volume - decreasing processes in the liquid cavity as well as the movement of the differential-area piston. These processes and the corresponding relationship will be analyzed, whereas the PAT dynamic model establishment is presented as follows.

The pressure and density equations of the gas cavity are given as follows

$$\frac{\mathrm{d}p_{\mathrm{g}}}{\mathrm{d}t} = \frac{k}{V_{\mathrm{g}}}\left[\left(puA\right)_{\mathrm{in}} - p_{\mathrm{g}}\frac{\mathrm{d}V_{\mathrm{g}}}{\mathrm{d}t} + \frac{k-1}{k}\frac{\mathrm{d}Q_{\mathrm{T,g}}}{\mathrm{d}t}\right] \quad (6)$$

$$\frac{\mathrm{d}\rho_{\mathrm{g}}}{\mathrm{d}t} = \frac{1}{V_{\mathrm{g}}}\left(puA\right)_{\mathrm{in}} - \frac{\rho_{\mathrm{g}}}{V_{\mathrm{g}}}\frac{\mathrm{d}V_{\mathrm{g}}}{\mathrm{d}t} \quad (7)$$

where

$$\frac{\mathrm{d}Q_{\mathrm{T,g}}}{\mathrm{d}t} = h_{\mathrm{s,g}}S\left(T_{\mathrm{w,g}} - T_{\mathrm{g}}\right) \quad (8)$$

The pressure of the liquid cavity is expressed as

$$\frac{\mathrm{d}p_{\mathrm{l}}}{\mathrm{d}t} = \frac{a_{\mathrm{l}}^{2}}{V_{\mathrm{l}}}\left[-\left(puA\right)_{\mathrm{out}} - p_{\mathrm{l}}\frac{\mathrm{d}V_{\mathrm{l}}}{\mathrm{d}t}\right] \quad (9)$$

The piston motion equations are

$$m_{\mathrm{pst}}\frac{\mathrm{d}u_{\mathrm{pst}}}{\mathrm{d}t} = F_{\mathrm{f}} + p_{\mathrm{g}}A_{\mathrm{g}} - p_{\mathrm{l}}A_{\mathrm{l}} - p_{\mathrm{a}}A_{\mathrm{pst}} \quad (10)$$

$$\frac{\mathrm{d}x_{\mathrm{pst}}}{\mathrm{d}t} = u_{\mathrm{pst}} \quad (11)$$

Due to the piston moving, the volume in the gas and liquid cavities are continuously changing, and can be expressed as follows

$$\frac{\mathrm{d}V_{\mathrm{g}}}{\mathrm{d}t} = A_{\mathrm{g}}u_{\mathrm{pst}} \quad (12)$$

$$\frac{\mathrm{d}V_{\mathrm{l}}}{\mathrm{d}t} = -A_{\mathrm{l}}u_{\mathrm{pst}} \quad (13)$$

As presented in Fig.5, the LR can be simplified as a diaphragm with a spring, an inlet cavity and an outlet cavity.

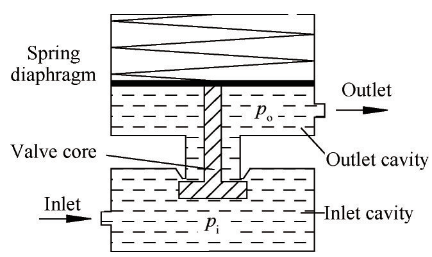

Fig. 5 Schematic diagram of the liquid regulator

According to the force balance, the valve core displacement equation is expressed as follows

$$m_{\mathrm{regc}}\frac{\mathrm{d}^2 l_{\mathrm{reg}}}{\mathrm{d}t^2} = C\frac{\mathrm{d}l_{\mathrm{reg}}}{\mathrm{d}t} - Kl_{\mathrm{reg}} + Kl_{\mathrm{reg0}} - p_{\mathrm{i}}A_{\mathrm{i}} - p_{\mathrm{o}}A_{\mathrm{o}} + p_{\mathrm{a}}A_{\mathrm{a}} \quad (14)$$

The mass flow of the regulator valve port is given below

$$q_{\mathrm{m,reg}} = C_{\mathrm{d,reg}}c_{\mathrm{reg}}l_{\mathrm{reg}}\sqrt{2\rho_{\mathrm{l}}\left(p_{\mathrm{o}} - p_{\mathrm{i}}\right)} \quad (15)$$

The GG is composed of a catalyst bed and an injector with capillaries. In the catalyst bed, the hydrazine 70 is completely decomposed, and the dissociation degree of ammonia is taken as 0.55. With consideration of the GG as a lumped parameters model, the mass conservation and the energy conservation equations for the combustor of the GG are given as follows

$$V_{\mathrm{GG}}\frac{\mathrm{d}\rho_{\mathrm{GG}}}{\mathrm{d}t} = q_{\mathrm{m,in,GG}} - q_{\mathrm{m,out,GG}} \quad (16)$$

$$\frac{\mathrm{d}p_{\mathrm{GG}}}{\mathrm{d}t}=\frac{k-1}{V_{\mathrm{GG}}}\left(h_{\mathrm{in,GG}}q_{\mathrm{m,in,GG}}-h_{\mathrm{out,GG}}q_{\mathrm{m,out,GG}}\right) \tag{17}$$

The catalyst bed and the capillary flow resistances are classified as local losses. The capillary flow resistance is presented below[13]

$$p_{\mathrm{in,cpl}}-p_{\mathrm{out,cpl}}=0.5\rho_1 u_{\mathrm{cpl}}^{\ 2}\left(H_{\mathrm{cpl}}+\frac{0.3164L_{\mathrm{cpl}}}{Re_{\mathrm{cpl}}^{\ 0.25}d_{\mathrm{cpl}}}\right) \tag{18}$$

where the flow resistance coefficient of capillary $H_{\mathrm{cpl}}=1.5$.

The catalyst bed flow resistance is expressed as follows[14]

$$\Delta p_{\mathrm{cb}}=2.157\times10^5\frac{a_{\mathrm{s}}^{1.2}G_{\mathrm{b}}^{1.8}L_{\mathrm{cb}}}{\varepsilon^{1.7}p_{\mathrm{GG}}},\ \text{while } Re_{\mathrm{c}}<600 \tag{19}$$

$$\Delta p_{\mathrm{cb}}=3.752\times10^5\frac{a_{\mathrm{s}}G_{\mathrm{b}}^{2}L_{\mathrm{cb}}}{\varepsilon^{1.7}p_{\mathrm{GG}}},\ \text{while } Re_{\mathrm{c}}\geqslant600 \tag{20}$$

The starting time can be defined as follows: when the differences among the PAT gas cavity pressure, the PT pressure and the self-locking gas pressure are within the allowable deviation, this moment can be set to the finishing moment of the starting process, whereas the time from the start to this moment can be defined as the starting time. This relationship is given as follows

$$\text{while}\begin{cases}\left|p_{\mathrm{g}}-p_{\mathrm{PT}}\right|<\Delta p_1\\ \left|p_{\mathrm{PT}}-p_{\mathrm{g,off}}\right|<\Delta p_2\end{cases},\ t_{\mathrm{st}}=t \tag{21}$$

2.2.2 Centroid drift evaluation

The gravity on the particles of the system can be observed as a parallel force system, where the corresponding center is the system centroid. For DPWGSPS, the centroid can be analyzed and calculated in the radial and axial directions on the basis of symmetry. Depending on the system components being treated as particles, the system coordinate origin is determined, whereas the system coordinates can be calculated by the following equations

$$x_{\mathrm{r}}=\frac{\sum M_i x_{\mathrm{r},i}}{\sum M_i} \tag{22}$$

$$x_{\mathrm{a}}=\frac{\sum M_i x_{\mathrm{a},i}}{\sum M_i} \tag{23}$$

The system axial direction is taken as the example to calculate the centroid drift. It can be supposed that the system initial mass is M_0 and the initial axial coordinate of the centroid is $x_{\mathrm{a},0}$. Subsequently to the operation of DPWGSPS, most liquid monopropellant is converted into warm gas and left from the DPWGPS to the propellant tank, the system mass becomes M_{F} and the axial coordinate of the centroid drifts to $x_{\mathrm{a,F}}$.

$$M_{\mathrm{F}}x_{\mathrm{a,F}}-M_0x_{\mathrm{a},0}=\sum^{n_i}\left(\Delta M_i\cdot x_{\mathrm{a},i}\right)+\sum^{n_j}\left(M_j\cdot\Delta x_{\mathrm{a},j}\right) \tag{24}$$

For the DPWGSPS, following the corresponding operation, the mass of the PAT, the liquid pipe, the gas pipe, the GG and the SC changed; the axial displacement of the piston of PAT occurred. The mass changes of the liquid and the gas cavity of PAT are presented as follows

$$\Delta M_{\mathrm{PAT,l}}=-\xi m_{\mathrm{mop}} \tag{25}$$

$$\Delta M_{\mathrm{PAT,g}}=\rho_{\mathrm{g}}V_{\mathrm{PAT,g,F}} \tag{26}$$

The mass change of the SC is

$$\Delta M_{\mathrm{SC}}=-m_{\mathrm{p}}+\rho_{\mathrm{g}}V_{\mathrm{SC}} \tag{27}$$

The mass changes of the liquid pipe, the gas pipe, the catalyst bed of the GG are presented as follows (ignoring the initial mass of the internal gas)

$$\Delta M_{\mathrm{pi,l}}=\rho_1V_{\mathrm{pi,l}} \tag{28}$$

$$\Delta M_{\mathrm{pi,g}}=\rho_{\mathrm{g}}V_{\mathrm{pi,g}} \tag{29}$$

$$\Delta M_{\mathrm{GG}}=\varepsilon\rho_{\mathrm{g}}V_{\mathrm{GG}} \tag{30}$$

Displacement change of PAT piston is

$$\Delta x_{\mathrm{pst}}=\xi L_{\mathrm{PAT,l}} \tag{31}$$

To sum up, the mass change of DPWGSPS following operation is

$$\begin{aligned}\Delta M=\Delta M_{\mathrm{SC}}+\Delta M_{\mathrm{PAT,g}}+\Delta M_{\mathrm{PAT,l}}+\\ \Delta M_{\mathrm{pi,l}}+\Delta M_{\mathrm{pi,g}}+\Delta M_{\mathrm{GG}}\end{aligned} \tag{32}$$

According to the previous equation

$$\begin{aligned}&\Delta x_{\mathrm{a}}=x_{\mathrm{a},F}-x_{\mathrm{a},0}=\\ &\frac{\sum^{n_i}\left(\Delta M_i\cdot x_{\mathrm{a},i}\right)+\sum^{n_j}\left(M_j\cdot\Delta x_{\mathrm{a},j}\right)-\Delta M\cdot x_{\mathrm{a},0}}{M_0+\Delta M}\end{aligned} \tag{33}$$

The axial centroid drift of the system is

$$\begin{aligned}\Delta x_{\mathrm{a}}=&\frac{1}{M_0+\Delta M}\Big[x_{\mathrm{a,SC}}\cdot\Delta M_{\mathrm{SC}}+\Delta x_{\mathrm{a,pst}}\cdot M_{\mathrm{pst}}+\\ &x_{\mathrm{a,PAT}}\cdot\left(\Delta M_{\mathrm{PAT,g}}+\Delta M_{\mathrm{PAT,l}}\right)+x_{\mathrm{a,pi,l}}\cdot\Delta M_{\mathrm{pi,l}}+\\ &x_{\mathrm{a,pi,g}}\cdot\Delta M_{\mathrm{pi,g}}+x_{\mathrm{a,GG}}\cdot\Delta M_{\mathrm{GG}}-\Delta M\cdot x_{\mathrm{a},0}\Big]\end{aligned} \tag{34}$$

The radial centroid drift of the system Δx_{r} has the same calculation method as the axial centroid drift Δx_{a}. The centroid drift of the system Δx is

$$\Delta x=\sqrt{\left(\Delta x_{\mathrm{a}}\right)^2+\left(\Delta x_{\mathrm{r}}\right)^2} \tag{35}$$

2.2.3 Pressurization efficiency estimation

With consideration to the surplus of the monopropellant in PAT and the liquid pipeline, as well as the surplus of warm gas in gas pipeline, only a portion of the monopropellant can be converted into pressurizing warm gas and left from DPWGSPS to the propellant tank. The pressurization efficiency η of DPWGSPS can be defined as the mass ratio of warm gas flowing into the propellant tank and the initial monopropellant mass.

$$\eta = \frac{M_{\mathrm{PT,g}}}{m_{\mathrm{mop}}} \tag{36}$$

2.3 Mass evaluation

The mass is an important index of DPWGSPS. The decrement of system mass is beneficial to the payload increase of the engine power system and to improve the operational capability. The establishment of the mass calculation model can include the methods of stress analysis, statistical regression or direct evaluation.

2.3.1 Mass of SC

The gross mass of the SC is calculated as

$$m_{\mathrm{SC}} = m_{\mathrm{SC,w}} + m_{\mathrm{p}} \tag{37}$$

$$m_{\mathrm{SC,w}} = m_{\mathrm{SC,tub}} + m_{\mathrm{SC,bot}} \tag{38}$$

where

$$m_{\mathrm{SC,tub}} = \rho_{\mathrm{SC,w}} \delta_{\mathrm{SC,tub}} \pi d_{\mathrm{SC}} L_{\mathrm{SC}} \tag{39}$$

$$m_{\mathrm{SC,bot}} = 2 \cdot \rho_{\mathrm{SC,w}} \delta_{\mathrm{SC,bot}} \frac{\pi}{4} d_{\mathrm{SC}}^2 \tag{40}$$

2.3.2 Mass of PAT

The PAT consists of the gas cavity tubular section, the liquid cavity tubular section, the gas cavity ellipsoidal head, the liquid cavity ellipsoidal head, the piston and the monopropellant.

The gross mass of the PAT is calculated as

$$m_{\mathrm{PAT}} = m_{\mathrm{eh,g}} + m_{\mathrm{tub,g}} + m_{\mathrm{eh,l}} + m_{\mathrm{tub,l}} + m_{\mathrm{pst}} + m_{\mathrm{mop}} \tag{41}$$

where

$$m_{\mathrm{eh}} = \rho_{\mathrm{PAT,w}} \delta_{\mathrm{eh}} S_{\mathrm{eh}} \tag{42}$$

$$m_{\mathrm{tub}} = \rho_{\mathrm{PAT,w}} \delta_{\mathrm{tub}} \pi d_{\mathrm{g}} L_{\mathrm{g}} \tag{43}$$

The area of the ellipsoidal head is

$$S_{\mathrm{eh}} = a^2 + \frac{\pi b^2 \ln\left[\frac{1+e}{1-e}\right]}{2e} \tag{44}$$

where e is the eccentricity ratio and $e = \frac{\sqrt{a^2 - b^2}}{a}$, a is the long inner radius of the ellipsoidal head, which is the same as the inner radius of the tubular section, b is the short inner radius of the ellipsoidal head; $d = 2a$.

2.3.3 Mass of GG

The mass of the GG includes the mass of the injector, the catalyst bed wall and the catalyst.

$$m_{\mathrm{GG}} = m_{\mathrm{inj}} + m_{\mathrm{cb}} + m_{\mathrm{ctl}} \tag{45}$$

The structure of the GG injector can be simplified as two planks; therefore, the mass of the injector is the sum of two planks. The injector and the catalyst bed are connected by the capillary, whereas a plank exists at the joint of the catalyst bed and the capillary; in order to conduct an easy calculation, the mass of the plank is included in the injector. Consequently, the injector mass is the sum of three plank masses, calculated as

$$m_{\mathrm{inj}} = 3\rho_{\mathrm{GG,w}} \delta_{\mathrm{inj,bot}} \frac{\pi}{4} d_{\mathrm{GG}}^2 \tag{46}$$

The mass of catalyst bed wall is

$$m_{\mathrm{cb}} = m_{\mathrm{cb,tub}} + m_{\mathrm{cb,co}} \tag{47}$$

where

$$m_{\mathrm{cb,tub}} = \rho_{\mathrm{GG,w}} \delta_{\mathrm{cb,tub}} \pi d_{\mathrm{GG}} L_{\mathrm{cb}} \tag{48}$$

$$m_{\mathrm{cb,co}} = \rho_{\mathrm{GG,w}} \delta_{\mathrm{cb,co}} \pi \frac{d_{\mathrm{GG}}^2 - d_{\mathrm{out}}^2}{\sin\alpha} \tag{49}$$

where α is the half angle of the cone at the GG outlet.

The mass of the catalyst is

$$m_{\mathrm{ctl}} = \rho_{\mathrm{ctl}} V_{\mathrm{cb}} (1 - \varepsilon) \tag{50}$$

2.3.4 Mass of pipe

$$m_{\mathrm{pi}} = \rho_{\mathrm{pi}} \delta_{\mathrm{pi,tub}} \pi d_{\mathrm{pi}} L_{\mathrm{pi}} \tag{51}$$

Through the stress analysis method, the thickness of the tubular wall, the flat bottom wall, the cone wall and the ellipsoidal wall are calculated as

$$\delta_{\mathrm{tub}} = \frac{pd}{2[\sigma]\phi - p} \tag{52}$$

$$\delta_{\mathrm{bot}} = d\sqrt{\frac{Kp}{[\sigma]\phi}} \tag{53}$$

$$\delta_{\mathrm{co}} = \frac{pd}{2[\sigma]\phi - p} \cdot \frac{1}{\cos\alpha} \tag{54}$$

$$\delta_{\mathrm{eh}} = \frac{K_{\mathrm{eh}} pd}{2[\sigma]\phi - 0.5p} \tag{55}$$

where K is the structure characteristic coefficient, K_{eh} is the shape coefficient of the ellipsoidal head, and $K_{\mathrm{eh}} = \frac{1}{6}\left[2 + \left(\frac{a}{b}\right)^2\right]$, ϕ is the welding joint coefficient.

2.3.5 Mass of other components

As for other modules such as the LR, the CV and the burst disks, the corresponding masses can be confirmed through a statistical method or direct evaluation according to the system characteristics, and the mass of these components can be summarized as m_{oth}.

The system total mass is the sum of the mass of each component

$$M = m_{SC} + m_{PAT} + m_{GG} + \sum m_{pi} + m_{oth} \quad (56)$$

3 Design optimization of DPWGSPS

3.1 Optimization objectives

For the DPWGSPS, the system total mass, the starting time, the centroid drift, the pressurization efficiency, the axial dimension and the radial dimension are important parameters. As a pressurization system for the propulsion system applied to missiles or spacecraft, the system total mass is the most important parameter of the system, and the response time (starting time) is the key performance parameter that is focused on. So, in current study, the system total mass and the starting time are chosen as the system-optimized two objectives in the multi-objective optimization. In some cases, if a parameter of the system is the target that needs to be considered separately, then it can be selected as the single objective for the system optimization. Consequently the optimization objective can be selected for one as minimization of the system total mass, the starting time, the centroid drift, the axial dimension and the radial dimension, as well as to the maximization of pressurization efficiency.

3.2 Optimization design variables and constraints

For DPWGSPS, the system variables can be classified as the important variables and normal variables, or the dependent variables and independent variables. The important and independent variables have strong impacts on the system performance, which can be selected as the design variables, such as the PAT liquid cavity diameter, the piston friction, the initial volume of the PAT gas cavity, the stressed area of the valve core in the LR inlet cavity, the stressed area of the valve core in the LR inlet cavity, the spring stiffness, the pressure drop of LR, the capillary length and the solid propellant mass of SC, etc.

The constraints are selected according to the system requirements. As an example, when the optimization objectives are the minimizations of the system total mass and starting time, the constraints can be selected from the centroid drift, the pressurization efficiency, the axial dimension and the radial dimension.

3.3 Optimization models

The multi-objective constrained optimization model of the system parameters is presented as follows

$$\min \boldsymbol{F}(\boldsymbol{X}) = [M(\boldsymbol{X}), t_{st}(\boldsymbol{X})]$$
$$\text{s.t.} \begin{cases} \Delta x(\boldsymbol{X}) \leqslant \Delta x_{max} \\ \eta(\boldsymbol{X}) \geqslant \eta_{min} \\ L_a(\boldsymbol{X}) \leqslant L_{a,max} \\ L_r(\boldsymbol{X}) \leqslant L_{r,max} \\ L_b \leqslant \boldsymbol{X} \leqslant U_b \end{cases} \quad (57)$$

where, $\boldsymbol{F}(\boldsymbol{X})$ is the objective functions, in this study, two objective functions is considered: one function minimized the system total mass and the other function minimized the starting time; η_{min}, Δx_{max}, $L_{a,max}$ and $L_{r,max}$ are respectively the lower limit of pressurization efficiency, the upper limit of centroid drift, the axial dimension and the radial dimension; L_b, U_b respectively represent the lower boundary and upper boundary vectors of the design variables; $\boldsymbol{X}$ is the design variables vector

$$\boldsymbol{X} = \left[d_1, F_f, V_{g0}, A_i, A_o, K, \Delta p_{reg}, L_{cpl}, m_p \right]^T \quad (58)$$

In this study, the single-objective optimizations is also investigated. The purpose of these works are to obtain the optimal values of each system parameters in the absence of constraints (except for the range of variable values), as well as other features, for providing support for the system design. The single-objective optimization model of the system parameters is presented as follows

$$\begin{aligned} &\min \boldsymbol{F}(\boldsymbol{X}) \\ &\text{s.t.}\ \boldsymbol{L}_b \leqslant \boldsymbol{X} \leqslant \boldsymbol{U}_b \end{aligned} \quad (59)$$

where, $\boldsymbol{F}(\boldsymbol{X})$ is single-objective function, which is defined as the fitness function of the system total mass, the starting time, the centroid drift, the pressurization efficiency, the axial dimension or the radial dimension.

3.4 Optimization methods

If the system optimization model is a multi-objective constrained optimization problem, which can be solved through the method presented in Fig.6. This problem can be converted into an optimization which has single objective and no constraint.

The most common approach to multi-objective optimization is the weighted sum method[15]. The transformation objective function $\boldsymbol{F}(\boldsymbol{X})$ is presented as

$$\min \boldsymbol{F}(\boldsymbol{X}) = \sum_{i=1}^{n_f}\left(\omega_i\left|\frac{f_i(\boldsymbol{X})}{f_{0,i}(\boldsymbol{X})}\right|\right) \tag{60}$$

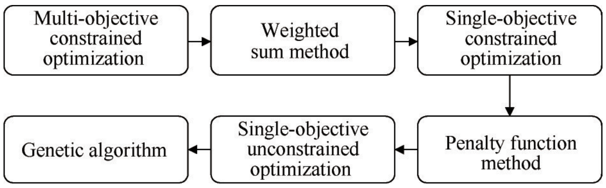

Fig. 6 Optimization mathematical method of DPWGSPS

where, $f_{0,i}(\boldsymbol{X})$ is the average value of the change of the design objective i, n_f is the number of functions $f(\boldsymbol{X})$. According to this, the multi-objective optimization is converted into single-objective optimization. The weighted factor ω_i is put forward based on relative important degrees of each objective function, and $\sum\omega_i = 1$. If all weighted factors are positive, the minimum of (59) is the Pareto optimal[16].

As for the inequality constraint, according to the penalty function method[17], it can be obtained as

$$\boldsymbol{F}\left(\boldsymbol{X},\sigma^{(k)}\right) = \boldsymbol{F}(\boldsymbol{X}) + \sigma^{(k)}\sum_{i=1}^{n_g}\left[\max\left(0,-g_i(\boldsymbol{X})\right)\right]^2 \tag{61}$$

where $\sigma^{(k)}$ indicates the penalty coefficient, which is a positive increasing sequence, $g_i(\boldsymbol{X})$ is the i th constraint function. n_g is the number of functions $g(\boldsymbol{X})$. Therefore, $\boldsymbol{F}\left(\boldsymbol{X},\sigma^{(k)}\right)$ is the augmented objective function. The original constraint problem is transformed into the unconstrained problem.

Genetic algorithms are stochastic optimization methods based on concepts of natural selection and genetics. They work with a population of individuals, each individual representing a possible result for a given problem. Genetic algorithm is used to solve the optimization problem. The flow chart of design optimization for DPWGSPS based on genetic algorithm is presented in Fig.7.

The system total mass optimization is taken as the example to explain the optimization process with the genetic algorithm. The parameters are set as follows: population size of 100, maximum number of generations of 100, crossover rate of 0.99 and mutation rate of 0.2. For regrouping the population $\boldsymbol{X}$, the percentage of the previous generation $\boldsymbol{X}$, the genetic population $\boldsymbol{X}_1$ and the new population $\boldsymbol{X}_2$ are set at 20%, 20% and 60%, respective-

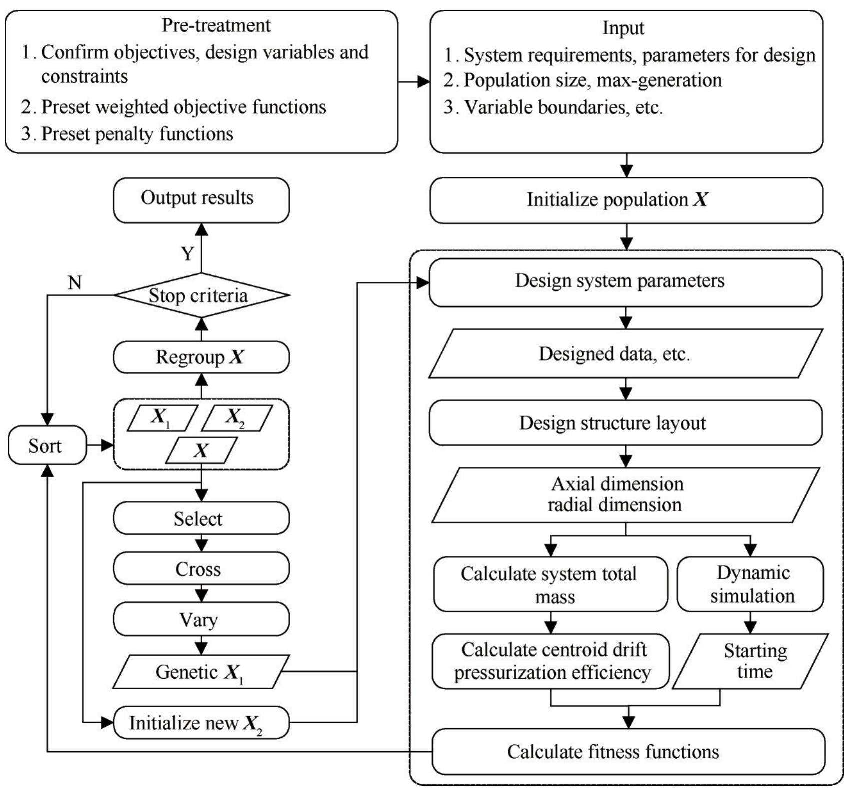

Fig. 7 Flow chart of design optimization for DPWGSPS

ly. According to Fig.8 ~ 10, the initial generation is generated through the random method and has strong individual dispersion, which facilitates a global search. When it is evolved to the 5th generation, the essential framework formed and the previous 40 values of the population are in-between 1.296 and 1.300kg, which are close to the optimal value. When evolved to the last generation (the 100th generation), the previous 40 values are all equal to the optimal value of 1.290kg. It can be observed from Fig. 11 that the value of total mass has converged to the corresponding optimal value, when it evolved to the 30th generation. As aforementioned, it is demonstrated that the genetic algorithm and the parameter setting has reliable astringency and well precision.

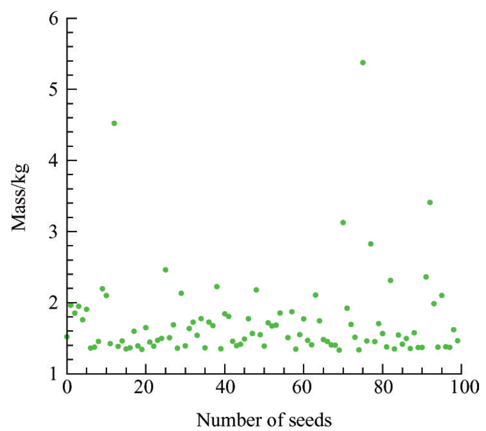

Fig. 8 First generation population distribution

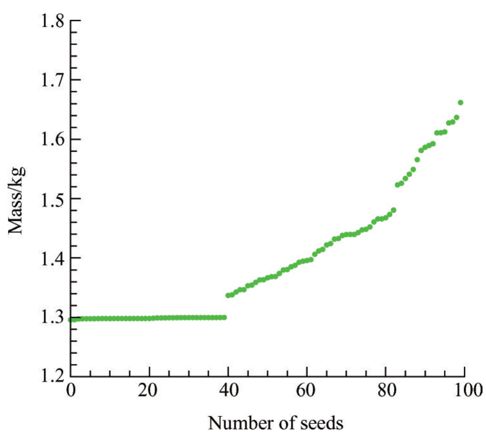

Fig. 9 Fifth generation population distribution

4 Results and discussion

4.1 Design variables on system parameters

Based on the system parameter calculation models, in this part, an investigation of the key design variables effects of DPWGSPS (d_l, F_f, V_{g0}, A_i, A_o, K, Δp_{reg}, L_{cpl}, m_p) on the system parameters (M, t_{st}, Δx, η, L_a, L_r) are described. Some design variables effects on the system parameters are presented in Fig. 12, and for DPWGSPS, the percentage data of the system parameters changed with the design variables in the corresponding feasible range presented in Table 1.

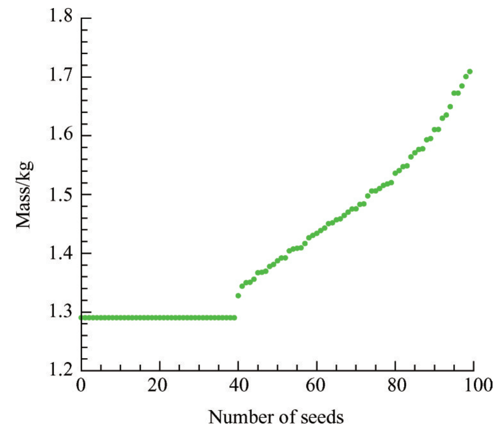

Fig. 10 Last generation population distribution

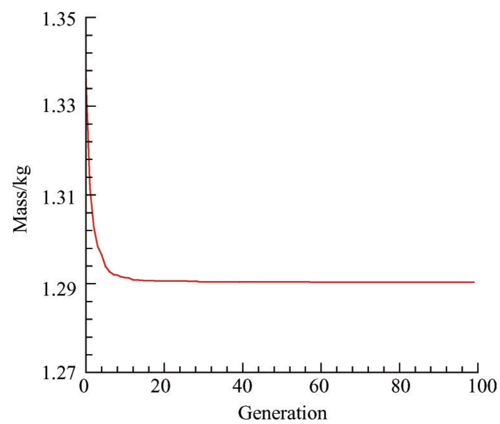

Fig. 11 Evolution process of objective function

It can be known from Fig.12 (a) and (b) that within the feasible range, as the d_l increased, the M increased to 56.74%; the t_{st} decreased at first and consequently increased; the Δx decreased at first, consequently increased and finally decreased; the increase of η is indistinctive (only 0.16%), the change of L_a is −60.92%, and L_r has the most extreme change of 141.6%.

According to Fig.12(c), as the V_{g0} increased, the M decreased; the t_{st} increased at first and consequently decreased; the Δx decreased at first, consequently increased and finally decreased; all changed highly, respectively as 160.67%, 141.42% and 210.42%.

From Fig. 12(d), as the m_p increased, the M remained unchanged at first, consequently decreased 41.89%; the t_{st} decreased at first and consequently increased with a change of 387.41%. The Δx is unchanged at first and consequently decreased 221.25%. The reason for certain parameters to remain unchanged at first is that when the solid propellant mass of SC is below a specific value, (which is 1.93g in the figure), the maximum pressure of PAT is decided on the self-locking pressure; when this value is exceeded, it is dependent on the starting pressure, which is affected by the solid propellant mass of SC.

As presented in Table 1, the system total mass is mainly affected by the initial volume of the PAT gas cavity, the PAT liquid cavity diameter and the solid propellant mass of SC, which exceeded 40%. Through the size and maximum operation pressure of the PAT, these parameters determine the PAT mass, consequently affecting the system total mass. On the other hand, the system

Table 1　System parameters change with design variables (%)

Design variables		d_l/mm [60,150]	F_f/N [1500,2500]	V_{g0}/mL [10,100]	A_i/mm^2 [30,130]	A_o/mm^2 [500,1000]	K/(MN/m) [3.5,5.5]	Δp_{reg}/MPa [0.5,1.5]	L_{cpl}/mm [15.30]	m_p/g [1.5,3.5]
System parameters	M	56.74	1.08	160.67	0.15	0.38	0.06	5.46	0.90	41.89
	t_{st}	17.14	0.8	141.42	27.51	10.43	10.20	3.00	6.11	387.41
	Δx	14.83	4.04	210.42	2.27	4.08	0.87	5.40	6.85	221.25
	η	0.16	0.10	0.33	0	0	0	0.26	0.05	0
	L_a	60.92	0.07	4.24	0	0	0	0.19	2.60	0
	L_r	141.67	1.95	0	0	0	0	5.52	0.80	0

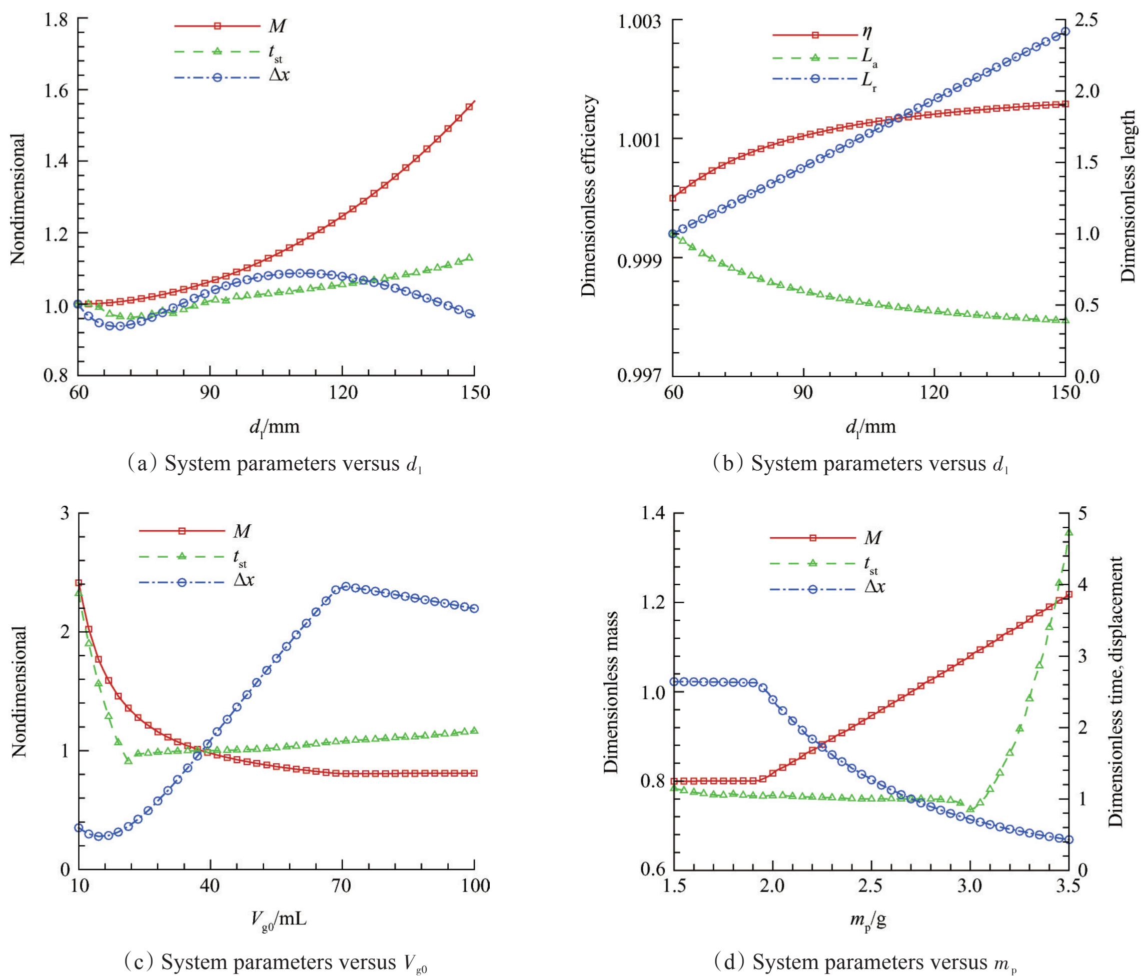

(a) System parameters versus d_l　(b) System parameters versus d_l

(c) System parameters versus V_{g0}　(d) System parameters versus m_p

Fig. 12　Effects of design variables on system parameters

total mass is also affected by the pressure drop of LR, which is beyond 5%. The pressure drop of LR affects the system mass by affecting the pressure distribution and the liquid self-locking pressure. A slight effect (less than 0.4%) originated by the stressed area of the valve core in the LR inlet cavity, the stressed area of the valve core in the LR outlet cavity, and the spring stiffness.

The starting time is mainly affected (beyond 140%) by the solid propellant mass of SC and the initial volume of the PAT gas cavity, which directly decided the starting pressure. This also depends on the diameter of the PAT liquid cavity, the stressed area of the valve core in the LR inlet cavity and outlet cavity, the spring stiffness, the capillary length and the pressure drop of LR, which affected by lower than 3%. Also, the friction of the piston affects less, by lower than 1%.

The centroid drift is mainly caused by the piston movement and the monopropellant discharge, whereas the residual liquid and gas also affect the drift. The solid propellant mass of SC and the initial volume of the PAT gas cavity affect the piston mass through the gas cavity staring pressure, thereby creating a major effect on the centroid drift by the movement of the piston (beyond 210%). The PAT liquid cavity diameter has a direct effect on the PAT liquid cavity length, consequently affecting the centroid drift formed by the piston movement and the monopropellant discharge (below 15%). Other variables affect the centroid drift by affecting the residual liquid and gas in the system (below 7%).

The pressurization efficiency is simply affected by the PAT liquid cavity diameter, the piston friction, the initial volume of the PAT gas cavity, the pressure drop of LR and the capillary length. When the system pressurization efficiency is calculated, it is assumed that the discharge ratio of monopropellant from the PAT is 98%. Consequently, the pressurization efficiency is only affected by the residual liquid and gas in the system except the PAT liquid cavity. The mass change of the residual liquid and gas varied with the design variables within the corresponding feasible range, being far lower than the initial monopropellant mass; therefore, the change of the pressurization efficiency affected by the design variables is quite low (all below 0.35%).

The axial dimension is affected by the PAT liquid cavity diameter, the piston friction, the initial volume of the PAT gas cavity, the pressure drop of LR and the capillary length. The most important one is the PAT liquid cavity diameter, which effect is beyond 60%. This is because, in the aforementioned system layout, regardless of the pipe length effect, the PAT length plays a major role in the axial dimension of the system. Also, the PAT liquid cavity diameter change directly affects the PAT length, when the monopropellant mass is fixed.

The radial dimension is affected by the PAT liquid cavity diameter, the piston friction, the pressure drop of LR and the capillary length. The most important one is the PAT liquid cavity diameter, which effect is beyond 140%. According to system layout, the radial dimension is the PAT gas cavity diameter, which is determined by the PAT liquid cavity diameter and the area amplification ratio. The pressure drop of LR and the capillary length are the main factors affecting the pressure drop of the system, whereas the area amplification ratio is decided by the system pressure drop and the piston friction force through the pressure amplification ratio. Consequently, the radial dimension is mainly decided by the PAT liquid cavity diameter, being related to the other parameters forehand discussed.

4.2 Single-objective optimization

The lower boundary and upper boundary vectors of the design variables are set as

$$\begin{cases} \boldsymbol{L}_{\mathrm{b}} = [\,60, 1500, 10, 30, 500, 3.5, 0.5, 15, 1.5\,]^{\mathrm{T}} \\ \boldsymbol{U}_{\mathrm{b}} = [\,150, 2500, 100, 130, 1000, 5.5, 1.5, 30, 3.5\,]^{\mathrm{T}} \end{cases} \tag{62}$$

Regarding the minimizations of the system total mass, the starting time, the centroid drift, the axial dimension and the radial dimension, as well as the maximization of the pressurization efficiency as the optimization objective, respectively, the optimization results of the system parameters and the design variables are presented in Table 2 and Table 3.

When the single-objective function is the system total mass, the starting time, the centroid drift, the pressurization efficiency, the axial dimension or the radial dimension, the optimal values of each optimization object are 1.290kg, 0.490s, 1.258mm, 95.637%, 0.215m and 66.469mm, respectively.

The initial volume of the PAT gas cavity has no effect on the radial dimension. Also, the stressed area of the valve core in the LR inlet cavity, the stressed area of the valve core in the LR outlet cavity, the spring stiffness and the solid propellant mass of SC have no effect on the pressurization efficiency, the axial dimension and the radial dimension. Consequently, during the relevant objective optimization, the design variables forehand discussed can have any value in the feasible range. According to the previous tables, in any case of single-objective optimization, the stressed area of the valve core in the LR inlet cavity, the spring stiffness and the capillary length can be fixed as the upper boundary of feasible range (130mm) and the lower boundary of feasible range (3.5kN/m and 15mm).

Through the results of Table 2 and Table 4 comparisons, the system parameter changes subsequently to single-objective optimization can be observed in Table 5.

According to Table 5, when the system total mass, the starting time, the centroid drift, the pressurization efficiency, the axial dimension and the radial dimension are respectively regarded as objective, the optimization object can be optimized at 23.17%, 34.40%, 84.10%, 0.42%, 62.28% and 4.14%. The system total mass, the starting time, the centroid drift and the axial dimension can be optimized efficiently; the radial dimension and the pressurization efficiency changed slightly. The optimal result can be obtained through rational objective function selection.

According to the aforementioned results, the piston friction, the stressed area of the valve core in the LR inlet cavity, the spring stiffness, as well as the capillary length all have slight or no effect, or the monotonous effect on the system parameters; these variables can be set as fixed-value parameters in the optimization process, whereas the F_f, A_i, K and L_{cpl} can be respectively taken to the corresponding lower limit (1500N), upper limit (130 mm^2), lower limit (3.5MN / m) and lower limit (15.0mm) in the feasible range.

The theoretical best values for each system parameter can be obtained by these single-objective optimizations, however, these values cannot be achieved due to the existence of actual constraints and other objects, but they can provide a data reference for the design.

Table 2 System parameter results of single-objective optimization

Objectives		$M(X)$	$t_{st}(X)$	$\Delta x(X)$	$\eta(X)$	$L_a(X)$	$L_r(X)$
System parameters	M/kg	1.290	1.806	2.730	7.660	8.769	1.621
	t_{st}/s	0.651	0.490	1.554	1.481	1.356	0.740
	Δx/mm	19.766	6.298	1.258	7.633	7.820	8.067
	η/%	95.517	95.199	95.390	95.637	95.370	95.427
	L_a/m	0.470	0.477	0.560	0.215	0.215	0.565
	L_r/mm	74.661	78.642	67.866	161.667	172.160	66.469

Table 3 Design variable results of single-objective optimization

Objectives		$M(X)$	$t_{st}(X)$	$\Delta x(X)$	$\eta(X)$	$L_a(X)$	$L_r(X)$
Design variables	d_1/mm	67.86	67.47	60.00	150.00	150.00	60.00
	F_f/N	1500	1500	2500	1500	2500	1500
	V_{g0}/mL	21.0	39.0	23.0	10.0	10.0	[10.0,100.0]*
	A_i/mm^2	130.0	130.0	130.0	[30.0,130.0]*	[30.0,130.0]*	[30.0,130.0]*
	A_o/mm^2	500.0	1000.0	500.0	[500.0,1000.0]*	[500.0,1000.0]*	[500.0,1000.0]*
	K/(MN/m)	3.50	3.50	3.50	[3.50,5.50]*	[3.50,5.50]*	[3.50,5.50]*
	Δp_{reg}/MPa	0.50	1.50	0.50	0.50	1.50	0.50
	L_{cpl}/mm	15.00	15.00	15.00	15.00	15.00	15.00
	m_p/g	1.50	2.91	3.50	[1.50,3.50]*	[1.50,3.50]*	[1.50,3.50]*

Annotations: * represents internal without constraint

During the process of single-objective optimization, certain system parameters can be simultaneously improved, whereas others may be passively reduced. For instance, when the centroid drift, the pressurization efficiency and the axial dimension get optimized, the system total mass and starting time will be drastically reduced. In order to solve this problem, the multi-objective optimization can be considered.

Table 4 Initial value of system parameters

Parameters	M/kg	t_{st}/s	Δx/mm	η/%	L_a/m	L_r/mm
Values	1.679	0.747	7.914	95.241	0.570	69.341

4.3 Multi-objective constrained optimization

Through the optimization methods described above section, the two-objective constrained optimization can be changed to the single-objective unconstrained optimization, which is presented as

$$\min \boldsymbol{F}(\boldsymbol{X})=\sum_{i=1}^{n_f}\left(\omega_i\left|\frac{f_i(\boldsymbol{X})}{f_{0,i}(\boldsymbol{X})}\right|\right) \tag{63}$$

where, $\boldsymbol{F}(\boldsymbol{X})$ is the optimization objective function, ω_1 is the weight of system total mass, ω_2 is the weight of starting time; M_0 and $t_{st,0}$ are the average value of the change of the system total mass and starting time. From the aforementioned investigation, the values of the piston friction, the stressed area of the valve core in the LR inlet cavity, the spring stiffness and the capillary length can be set to fixed values, where F_f, A_i, K, L_{cpl} are respectively 1500N, 130mm^2, 3.5MN/m and 15.0mm; so

$$\begin{cases}\boldsymbol{X}=\left[d_1, V_{g0}, A_o, \Delta p_{reg}, m_p\right]^{T}\\ g_1(\boldsymbol{X})=\Delta x_{max}-\Delta x(\boldsymbol{X})\\ g_2(\boldsymbol{X})=\eta(\boldsymbol{X})-\eta_{min}\\ g_3(\boldsymbol{X})=L_{a,max}-L_a(\boldsymbol{X})\\ g_4(\boldsymbol{X})=L_{r,max}-L_r(\boldsymbol{X})\\ \boldsymbol{L}_b=[60,10,500,0.5,1.5]^{T}\\ \boldsymbol{U}_b=[150,100,1000,1.5,3.5]^{T}\end{cases} \tag{64}$$

where Δx_{max}, η_{min}, $L_{a,max}$, $L_{r,max}$ are respectively 100mm, 0.955, 350mm and 150mm.

In order to obtain the Pareto-frontier solutions to the minimization of the system total mass and the starting time, several groups of weighted factors are utilized to construct the problem. Therefore, the Pareto-frontier solution is presented in Fig.13.

The optimized results at different weighted factors and the deviations in comparison with the initial system parameters are presented in Table 6. According to Fig.13 and Table 6, the system total mass varies within [1.537kg, 2.533kg], when the weighted factor of the system total mass ω_1 is in the range of 1.0 to 0.0, the corresponding deviation falls within [−8.46, 50.86]; and the starting time varies within [0.521s, 0.722s], when the weighted factor of starting time ω_2 is in the range of 1.0

Table 5 System parameter changes of single-objective optimization (%)

Objectives		$M(X)$	$t_{st}(X)$	$\Delta x(X)$	$\eta(X)$	$L_a(X)$	$L_r(X)$
System parameters	M	−23.17	7.56	62.60	356.22	422.28	−3.45
	t_{st}	−12.85	−34.40	108.03	98.26	81.53	0.94
	Δx	149.76	−20.42	−84.10	−3.55	−1.19	1.93
	η	0.29	−0.04	0.16	0.42	0.14	0.20
	L_a	−17.54	−16.32	−1.75	−62.28	−62.28	−0.88
	L_r	7.67	13.41	−2.13	133.15	148.28	−4.14

Table 6 Optimized system parameters and deviations in comparison with initial values

Objectives	ω_1	1.0	0.9	0.8	0.7	0.6	0.5	0.4	0.3	0.2	0.1	0.1
	ω_2	0.0	0.1	0.2	0.3	0.4	0.5	0.6	0.7	0.8	0.9	1.0
$M(X)$	kg	1.537	1.556	1.562	1.580	1.597	1.620	1.671	1.810	1.991	2.103	2.533
	%	−8.46	−7.33	−6.97	−5.90	−4.88	−3.51	−0.48	7.80	18.58	25.25	50.86
$t_{st}(X)$	s	0.722	0.686	0.673	0.644	0.625	0.600	0.560	0.538	0.528	0.526	0.521
	%	−3.35	−8.17	−9.91	−13.79	−16.33	−19.68	−25.03	−27.98	−29.32	−29.59	−30.25

to 0.0, the corresponding deviation falls within [-3.35, -30.25]. Under the above constraints, the optimized starting times are all lower than the initial design value. When the weighted factor of the system total mass is in the range of 1.0 to 0.4, the system total mass can be optimized; otherwise, the mass is higher than the corresponding initial design value. When the weighted factor of starting time exceeded 0.6, the reducing of the starting time displays a decreasing trend and the increase of the system total mass displays an increasing trend, as the starting time weighted factor increased. Therefore, the combination objectives with the weighted factor of system total mass lower than 0.4 (or the weighted factor of starting time beyond 0.6) are not good objective options for the DPWGSPS. Consequently, in the two-objective optimization, it can be obtained from the optimized results that when the weighted factor of the system total mass varies within [0.4, 1.0] (or the weighted factor of starting time varies within [0.0, 0.6]), and the system total mass varies within [1.537kg, 1.671kg], the starting time varies within [0.560s, 0.722s]; these two weighted factors can be evaluated according to the system requirements.

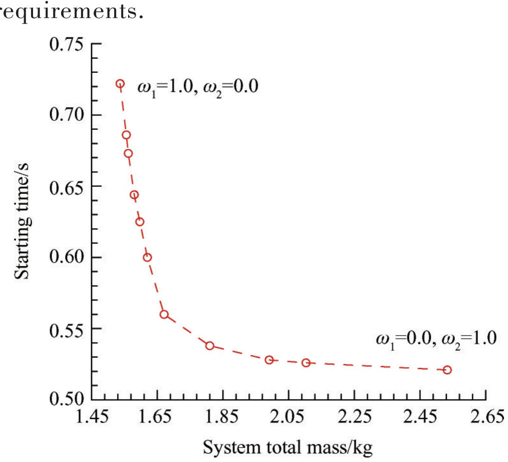

Fig. 13 Pareto frontier of preset optimization problem

5 Conclusions

According to the aforementioned studies, the main conclusions are as follows:

(1) The system total mass, the starting time, the centroid drift, the axial dimension and the radial dimension are mainly affected by the gas cavity initial volume of the pressure amplified tank, the liquid cavity diameter of the pressure amplified tank and the solid propellant mass of start cartridge; the pressurization efficiency change affected by the design variables is quite low. The piston friction, the stressed area of the valve core in the liquid regulator inlet cavity, the spring stiffness, the capillary length have slight or no effect, or a monotonous effect on the system parameters; and these variables can be respectively taken to the corresponding lower limit, upper limit, lower limit and lower limit in the feasible range.

(2) Through the selection of one of the system parameters as the single objective, the system total mass, the starting time, the centroid drift, the axial dimension and the radial dimension can be decreased by 23.17%, 34.40%, 84.10%, 62.28% and 4.14%, respectively, and the pressurization efficiency can increase 0.42%.

(3) For the multi-objective constrained optimization, the objective functions are the minimization of the system total mass as well as of the starting time, where the constraints are the other system parameters. From the optimization, the Pareto-frontier solution is obtained. The optimized results can be obtained while the weighted factor of the system total mass varies within [0.4, 1.0] (or the weighted factor of starting time varies within [0.0, 0.6]), and the system total mass varies within [1.537kg, 1.671kg], the starting time varies within [0.560s, 0.722s].

References:

[1] Maybee J C, David J K. A Novel Design Warm Gas Pressurization System [R]. *AIAA* 98-4014.

[2] 方忠坚，刘 洌，梁国柱. 差动活塞式燃气自增压系统参数设计方法[J]. 北京航空航天大学学报，2017，43(1): 61-70.

[3] 方忠坚，刘 洌，梁国柱. 差动活塞式热气自增压系统静态特性仿真研究[J]. 推进技术，2018，39(3): 538-546. (FANG Zhong-jian, LIU Lie, LIANG Guo-zhu. Simulation Research of Static Characteristics of Differential Piston Warm Gas Self-Pressurization System [J]. *Journal of Propulsion Technology*, 2018, 39(3): 538-546.)

[4] Liu L, Liang G Z. Optimization Selection of Regulated Pressurization System Schemes for Liquid Attitude and Divert Propulsion Systems [J]. *Procedia Engineering*, 2015, 99: 1247-1251.

[5] Cai G B, Tong X Y, Zheng Y T, et al. Generic Optimization of System Parameters for Liquid Rocket Engine

with Gas Generator Cycle [R]. *AIAA* 2005-3743.

[6] Cai G B, Fang J, Zheng Y T, et al. Optimization of System Parameters for Liquid Rocket Engine with Gas-Generator Cycles [J]. *Journal of Propulsion and Power*, 2010, 26(1): 113-119.

[7] Kosugi Y, Oyama A, Fujii K, et al. Multidisciplinary and Multi-Objective Design Exploration Methodology for Conceptual Design of a Hybrid Rocket[R]. *AIAA* 2011-1634.

[8] Oyama A, Liou M S. Multiobjective Optimization of Rocket Engine Pumps Using Evolutionary Algorithm [J]. *Journal of Propulsion and Power*, 2002, 18(3): 528-535.

[9] 郑赟韬，童晓艳，蔡国飙，等. 液体火箭发动机系统设计仿真与优化[J]. 北京航空航天大学学报，2006，32(1): 40-45.

[10] 张黎辉，凌桂龙，段 娜，等. 基于遗传算法的液体火箭发动机参数优化[J]. 航空动力学报，2008，23(5): 916-920.

[11] Pastrone D, Sentinella M R. Multi-Objective Optimization of Rocket-Based Combined-Cycle Engine Performance Using a Hybrid Evolutionary Algorithm[J]. *Journal of Propulsion and Power*, 2009, 25(5): 1140-1145.

[12] Liu K, Zhang Y L. A Study on Versatile Simulation of Liquid Propellant Rocket Engine Systems Transients [R]. *AIAA* 2000-3771.

[13] 周汉申. 毛细管流量系数实验研究[J]. 推进技术，1993，14(1): 34-39. (ZHOU Han-shen. Experiment on Capillary Flow Coefficient[J]. *Journal of Propulsion Technology*, 1993, 14(1): 34-39.)

[14] 朱宁昌，刘国球，董锡鉴，等. 液体火箭发动机设计[M]. 北京：中国宇航出版社，2005.

[15] Marler R, Arora J. Survey of Multi-Objective Optimization Methods for Engineering [J]. *Structural and Multidisciplinary Optimization*, 2004, 26: 369-395.

[16] Zadeh L. Optimality and Non-Scalar-Valued Performance Criteria [J]. *IEEE Transactions on Automatic Control*, 1963, 8(1): 59-60.

[17] Yeniay ö. Penalty Function Methods for Constrained Optimization with Genetic Algorithms [J]. *Mathematical and Computational Applications*, 2005, 10(1): 45-56.

（编辑：刘萝威）